Berbamine inhibits the infection of SARS-CoV-2 and flaviviruses by compromising TPRMLs-mediated endolysosomal trafficking of viral receptors

Lihong Huang
City University of Hong Kong
Huanan Li
Southeast Agricultural University of China
Terrence Tsz-Tai Yuen
University of Hong Kong
Zuodong Ye
City University of Hong Kong
Qiang Fu
City University of Hong Kong
Wei Sun
City University of Hong Kong
Qiang Xu
Southeast Agricultural University of China
Yang Yang
Shenzhen Third People's Hospital
Jasper Fuk-Woo Chan
University of Hong Kong
Guoliang Zhang
Shenzhen Third People's Hospital
Hin Chu (hinchu@hku.hk)
University of Hong Kong
Wenbao Qi (qiwenbao@scau.edu.cn)
Southeast Agricultural University of China
Jianbo Yue (yue.jianbo@cityu.edu.hk)
City University of Hong Kong

Research Article

Keywords: bis-benzylisoquinoline alkaloid, berbamine, (+)ss RNA viruses, SARS- CoV-2, JEV, ZIKV, DENV, Ca2+, TRPMLs, extracellular vesicles

Posted Date: May 26th, 2020

DOI: https://doi.org/10.21203/rs.3.rs-30922/v1

Abstract

Positive-sense single-stranded ((+)ss) RNA viruses are among the leading causes of human and animal infectious diseases in the world, but so far, no effective antiviral agents are available to treat these infections. Here we found that several bis- benzylisoquinoline alkaloids (e.g. berbamine), potently inhibited the infection of coronaviruses (e.g. SARS-CoV-2 and MERS-CoV), flaviviruses (e.g. JEV, ZIKV and DENV), and enteroviruses (e.g. EV-A71) in host cells. Moreover, berbamine protected mice from lethal challenge of JEV. We also found that berbamine inhibited TRPMLs (Ca2+ permeable non-selective cation channels in endosomes and lysosomes), which compromised the endolysosomal trafficking of viral receptors, such as ACE2 and DPP4. This led to the increased secretion of these receptors via extracellular vesicles and the concomitant decrease in their levels at the plasma membrane, thereby preventing (+)ss RNA viruses from entering the host cells. In summary, these results indicate that bis- benzylisoquinoline alkaloids such as berbamine, can act as a pan-anti-(+)ss RNA virus drug by inhibiting TPRMLs to prevent viral entry.

Introduction

Positive-sense single-stranded RNA viruses (also called (+)ss RNA viruses), include: coronaviruses (e.g. severe acute respiratory syndrome coronavirus 2 (SARS-CoV-2) and middle east respiratory syndrome coronavirus (MERS-CoV)); flaviviruses (e.g. Japanese encephalitis virus (JEV), Zika virus (ZIKV), and Dengue virus (DENV)); and enteroviruses (e.g. enterovirus A71 (EV-A71)). These viruses are a leading cause of human and animal infectious diseases around the world 1, 2, 3, 4, 5, 6, 7, 8, and the morbidity and mortality of the related diseases caused by these viruses have been a great burden for public health in recent years.

The infections of coronavirus cause a number of human and animal diseases, including infections of the gastrointestinal tract and upper respiratory system 9, 10, 11. Although majority of coronavirus infections are asymptomatic or mild, SARS-CoV is the causative for SARS outbreak in 2002 with a total of 8,098 cases and 774 fatalities (i.e. 9.6% of cases) 6, 7, 12, and MERS-CoV is the pathogen responsible for the outbreak of MERS, with fatality rate close to 35% 9, 13. We are currently being affected by coronavirus disease 2019 or COVID-19 due to infection by the SARS-CoV-2. So far, this has been transmitted around the world with more than 3 million cases of infection and a mortality rate close to 7%. COVID-19 has put much of the world into lockdown, and this public health emergency highlights the urgent need for the effective antiviral agents.

With regards to the common flaviviruses, DENV infects between 100 and 500 million people each year and causes about 50 million febrile illnesses, including more and more cases of hemorrhagic fever 1, 14. In contrast, a large proportion of ZIKV infections is asymptomatic and the main features of infected patients who do show symptoms include just mild fever, headache and arthralgia 15, 16, 17. However, the biggest concern with ZIKV, is the coincidence between the onset and rise of this viral infection and the increase in severe congenital infection leading to microcephaly in new-born babies reported in Brazil 16.

With regard to JEV, over the past few decades, various inactivated and living-attenuated forms of this virus have been successfully used for the production of vaccines in many countries, and the concomitant escalation in immunization programs has markedly decreased the burden of this disease. However, it has been estimated that annually JEV still affects about 68,000 people and results in 10,000-15,000 deaths, with 30%-50% of the survivors showing neurological sequelae 18, 19. The widespread global social and economic impact of flavivirus infection also urgently requires effective treatment interventions. However, so far, despite commercially available vaccines for yellow fever, Japanese encephalitis, and neonatal encephalitis, there is no effective clinical treatment for any flavivirus infection 4, 20.

EV-A71 is one of the most well-studied members of enterovirus family. EV-A71 easily spreads among children and may cause diarrhea, rashes, and hand, foot and mouth disease (HFMD), with the possibility of developing into severe neurological disease. Previously, many EV-A71 epidemics have taken place in Asian countries. For example, in 1998, there was a large EV-A71 outbreak in Taiwan, which led to the death of 78 children out of 405 hospitalized cases 21.

Ca2+ signaling plays role in almost every aspect of virus infection, from entry and replication, to packing and release 22, 23, 24, 25, 26, 27, 28, 29, 30. In addition, members of the transient receptor potential membrane channel mucolipin (TRPML) family, (Ca2+- permeable non-selective cation channels), are known to function in endolysosomal trafficking 31, 32. Here, we found that several bis-benzylisoquinoline alkaloids, especially berbamine, potently supressed the infection of many (+)ss RNA viruses, including SARS-CoV-2, MERS-CoV, JEV, ZIKV, DENV, and EV-A71, by inhibiting TRPMLs and thus preventing the entry of these viruses into the host cells.

Results

Ca2+ signaling is required for the entry of (+)ss RNA virus into host cells. It has been reported by a number of groups that Ca2+ signaling is essential for virus infection 22, 23, 24, 25, 26, 27, 28, 29, 30. Here, we added to this accumulating evidence by demonstrating that chelation of intracellular Ca2+ with BAPTA-AM markedly suppressed the JEV-induced expression of JEV envelope protein (JEV-E) (**Fig. 1A**). Since it has been reported that a Ca2+-dependent signaling pathway regulates the entry of the influenza A virus 27, 28, we subsequently studied if BAPTA-AM inhibits internalization of JEV. We performed *in situ* RNA hybridization to detect the positive strand RNA of JEV, the viral genome (vRNA), and showed that JEV was internalized as early as 20 min after infection, and a stronger vRNA signal was detected by 80 min after viral infection. However, when cells were treated with BAPTA-AM, no JEV vRNA was detected inside cells **(Fig. 1B)**. We also examined whether the removal of extracellular Ca2+ might affect ZIKV infection of host cells by performing both *in situ* RNA hybridization assay to detect the vRNA of ZIKV, and immunocytochemistry to investigate the localization of ZIKV envelope protein (ZIKV-E). We showed that at 90 min after viral infection, in the presence of extracellular Ca2+ ZIKV vRNA was detected inside host cells (middle panel in **Fig. 1C**), but in the absence of extracellular Ca2+, no ZIKV vRNA was detected

inside these cells (right panel in **Fig. 1C**). Moreover, in the absence of extracellular Ca2+, ZIKV virions, (manifested by ZIKV-E immunostaining), were detected at the plasma membrane of the host cells (right panel in **Fig. 1C**). These results indicate that Ca2+ signaling is required for the entry of (+)ss RNA viruses into host cells.

Berbamine inhibits JEV, ZIKV, DENV, SARS-CoV-2, and MERS-CoV infection in vitro. Double stranded RNAs (dsRNAs) are an intermediate in viral genome replication. They are generated by viral RNA polymerases following the infection of the (+)ss RNA viruses. These dsRNAs can be detected by performing immunofluorescence staining with an anti-dsRNA antibody 33, 34, 35. Thus, we used a combination of *in situ* RNA hybridization for the negative strand viral RNA ((-)RNA), and dsRNA immunostaining in the host cells to investigate the infection of the HeLa cells with EV-A71 or JEV. We found that 7h after virus infection, EV-A71 (-)RNA exhibited strong co-localization with dsRNA (**Fig. S1A**). DsRNA puncta were also detected in cells infected with JEV, and these puncta exhibited weak co-localization with EEA1 (an early endosome marker) or LAMP1 (a late endosome and lysosome marker) (**Fig. S1B**). This weak co-localization between dsRNA and endosomal or lysosomal markers suggests that for JEV, viral RNA replication does not occur at either the endosomes or lysosomes. Nevertheless, these results confirm that dsRNA immunostaining can be used to detect (+)ss RNA virus infection in host cells.

We, subsequently, developed a high-content image detection platform to detect and quantify the dsRNA immunostaining in virus-infected cells by automated fluorescence microscopy (**Fig. 2A**). We then applied this high-content image platform to assess the anti-viral activity of various compounds reported in the literature as being modulators of Ca2+ channels or Ca2+ signaling. Thus, A549 cells were seeded in 96-well plates, pretreated with different concentrations of various compounds for 1 h, and then infected with JEV, ZIKV or DENV. After 48 h of infection, the cells were fixed and subjected to dsRNA immunostaining and DAPI staining, after which images were captured with the CellInsight CX7 high-content screening platform and analyzed in HCS Studio™ 3.0 to quantify the percentage of infected cells (**Fig. 2A**).

By applying this high content image platform, we found that berbamine, a bis- benzylisoquinoline alkaloid isolated from the traditional Chinese medicine, Berberis, (which has reported effects on Ca2+ signaling), significantly inhibited the infection of JEV (**Fig. 2B**), ZIKV (**Fig. 2C**), and DENV (**Fig. 2D**). In A549 cells, the EC50 of berbamine against JEV and ZIKV was approximately 1.62 mM and 2.17 mM, respectively. Consistently, when we performed a virus titration assay, we could confirm that berbamine significantly inhibited the infectious progeny viral particle production of both ZIKV (**Fig. 2E**) and JEV (**Fig. 2F**). Taken together, these data not only demonstrate that berbamine is an effective anti-flavivirus agent, but also confirm the efficacy of our high-content image screening platform.

In addition to flaviviruses, we also assessed the activity of berbamine against coronavirus (e.g. MERS-CoV and SARS-CoV-2) infection *in vitro*. We treated primary human lung fibroblasts with berbamine and then infected them with MERS-CoV, after which we performed qRT-PCR to measure the amount of intra- or extracellular viral RNA. We showed that berbamine significantly decreased both the intracellular (**Fig. 3A**) and extracellular (**Fig. 3B**) level of MERs-CoV RNA. We also assessed the anti- SARS-CoV-2 activity of

berbamine in VeroE6 cells, and found that berbamine significantly inhibited the viral yield, as quantified by qRT-PCR (**Fig. 3C**). The EC50 of berbamine against SARS-CoV-2 in Vero cells is ~2.3 mM. In summary, these data indicate that in addition to being an effective anti-flavivirus agent, berbamine is also an effective anti-SARS-CoV-2 and MERS-CoV drug.

Analogues of berbamine also inhibit flavivirus and EV-A71 infection in vitro. In our screen of the different compounds, tetrandrine (a berbamine analogue isolated from *Stephania tetrandra* 36, 37, 38), also significantly inhibited JEV (**Fig. S2A** and **S2B**) and ZIKV (**Fig. S2C**) infection, as shown by our high content image assay. The EC50 of tetrandrine against JEV and ZIKV in A549 cells was ~1.73 mM and ~1.19 mM, respectively. Likewise, tetrandrine markedly inhibited the JEV infection-induced expression of JEV-NS1 in 4T1 cells (**Fig. S2D**), and significantly decreased the infectious progeny viral particle production of JEV (**Fig. S2E**) and ZIKV (**Fig. S2F**) in A549 cells.

In addition to berbamine and tetrandrine, we also assessed the ability of three additional bis-benzylisoquinoline alkaloids (i.e., isotetrandrine, fangchinoline, and E6 berbamine; **Fig. S3A**), to inhibit JEV or ZIKV infection of host cells. As shown in **Figs. S3B-S3D**, isotetrandrine, fangchinoline and E6 berbamine all significantly inhibited infection of JEV or ZIKV in host cells. Similarly, tetrandrine, isotetrandrine, and fangchinoline all significantly inhibited DENV2 infection in A549 cells in a concentration-dependent manner (**Fig. S4A**).

We also performed the high-content image assay to assess the effect of berbamine or tetrandrine on EV-A71 infection. As shown in **Figure S4B** and **S4C**, treatment with berbamine or tetrandrine significantly inhibited EV-A71 infection in RD cells, with EC50 values of ~17. 3 mM or ~7.6 mM, respectively. Taken together, these data indicate that these bis-benzylisoquinoline alkaloids act as pan anti-(+)ss RNA viral agents.

Berbamine can protect mice from a lethal challenge of JEV. We subsequently assessed the cytotoxicity of berbamine (**Fig. 4A**) and tetrandrine (**Fig. 4B**) in different cell lines, and found that the IC50 for berbamine in different cell lines ranged from ~90 μM to ~126 μM, whereas the IC50 of tetrandrine was from ~20 μM to ~28 μM (**Fig. 4C**). We also calculated the selectivity index (SI) of berbamine or tetrandrine for JEV and ZIKV infection. The SI helps to determine the window between cytotoxicity and antiviral activity by dividing the EC50 over its IC50 value (i.e., IC50/EC50). As shown in **Fig. 4D**, the SI values of berbamine were much higher than tetrandrine for these two viruses.

We, thus, assessed the protective effects of berbamine against JEV infection in a mouse model. As shown in **Figs. 4E** and **4F**, berbamine (15 mg/kg, twice per day) indeed protected mice from a lethal challenge of JEV, as demonstrated by the higher survival rate (i.e., 75% in the berbamine-treated group *versus* 12.5% in the control group) and the better body weight recovery. In summary, these results suggest that *in vivo*, berbamine is also a potential anti-(+)ss RNA viral drug or at least an anti-flaviviral drug.

Berbamine prevents the entry of (+)ss RNA viruses by decreasing the levels of their receptor(s) at the plasma membrane in host cells. Since chelation of intracellular Ca2+ by BAPTA-AM rendered cells

resistant to JEV internalization (**Fig. 1B**), we examined whether berbamine might block the entry of viruses into cells. Thus, A549 cells were treated with berbamine for 1h, and then then incubated with JEV on ice for 1h before putting back to 37 0C for another 80 min before fixation. *In situ* RNA hybridization was subsequently performed to detect the JEV vRNA. As expected, JEV vRNA was only detected in untreated control cells, and not in cells pretreated with berbamine or tetrandrine (**Fig. 5A**). Therefore, these data demonstrate that berbamine inhibits the entry of JEV into host cells.

We next investigated the mechanism by which berbamine prevents (+)ss RNA viruses from entering host cells, and focused on JEV. The early stages of the flavivirus life cycle involve the attachment of viral particles to the surface of the cell membrane. These viral particles bind to membrane receptors and then enter into the cell via receptor-mediated endocytosis, after which the viral RNA is released from the endosomes, due to the fusion of flavivirus E proteins with the endosome membrane. To search for potential JEV receptor(s) on host cells, we generated pools of siRNA, and individually knocked down potential virus receptors reported in the literature. In this way, we found that knockdown of the low-density lipoprotein receptor (LDLR) markedly decreased JEV-induced JEV-NS1 protein expression in A549 cells (**Fig. 5B** and **5C**), which suggests that the LDLR might be involved in JEV infection. The LDLR is a calcium binding protein, which has been reported to function as a receptor for the hepatitis C, rhino-, and vesicular stomatitis viruses 39, 40, 41, 42, 43. We then assessed whether LDLR is involved in JEV entry into cells. Thus, control or LDLR knockdown A549 cells were incubated with JEV on ice for 1h and were then incubated with warm medium at 37 0C for another 80 min followed by *in situ* RNA hybridization to detect the JEV vRNA. As expected, JEV vRNA was only detected in control cells, not in LDLR knockdown cells (**Fig. 5D**), indicating that LDLR is required for JEC entry. In addition, we incubated live A549 cells on ice with an anti-LDLR antibody and an Alexa Fluor 488-tagged secondary antibody to label the cell surface LDLR, followed by infection with JEV. Thereafter, cells were incubated at 37˚C, fixed at the indicated time points, and subjected to *in situ* RNA hybridization to detect the vRNA of the JEV (**Fig. 5E**). We showed that JEV infection induced the internalization of LDLR (green puncta in **Fig. 5E**), and the internalized LDLR-positive endosomes exhibited strong co- localization with the vRNA particles (red puncta in **Fig. 5E**) by 30 min after virus infection. The vRNA particles then became dissociated from the LDLR-positive endosomes by 60 min after virus infection (the lower panel in **Fig. 5E**), and we suspect that this is likely due to the release of viral genome RNA from the endosome. In addition, JEV infection markedly increased the level of LDLR in a time-dependent manner, whereas berbamine treatment abolished this increase (**Fig. 5F**). These results suggest that LDLR might be one of the receptors used by JEV to gain entry into the host cells, and berbamine decreases the level of LDLR at the plasma membrane thereby rendering cells refractory to JEV infection. We conducted LDLR immunostaining in cells treated with or without berbamine, and confirmed that in the presence of the drug, the level of LDLR at the plasma membrane was significantly decreased, but there was little effect on cell morphology (**Fig. 5G**).

Since SARS-CoV-2 and MERS-CoV are known to target ACE2 44 and DPP4 45, respectively, for their entry into host cells, we suspect that the anti-SARS-CoV-2 and anti-MERS-CoV activity of berbamine might also be due to its effect on these two receptors at the cell surface. By immunolabeling ACE2 or DPP4 in cells treated with or without berbamine, we showed that the drug indeed significantly decreased the level of

both of these receptor proteins at the plasma membrane (**Fig. 5H** and **5I**). In summary, these results suggest that berbamine prevents (+)ss RNA viruses from entering host cells by decreasing their respective receptors levels at the plasma membrane. *Berbamine inhibits endolysosomal trafficking and induces the secretion of extracellular vesicles to decrease viral receptor levels at the plasma membrane.* Since berbamine decreased the levels of LDLR at the plasma membrane (**Fig. 5F**), we assessed whether berbamine might affect the endolysosmal trafficking of LDLR by performing LDLR and LAMP1 co-immunostaining in cells treated with or without berbamine. In brief, A549 cells were first incubated with an anti-LDLR antibody on ice for 90 min. The internalization of the LDLR-antibody complex was then initiated when cells were warmed to 37°C 46. In the control cells, after ~30 min to 1 h the internalized LDLR- antibody complex was found in the late endosomes or lysosomes, as shown by the level of co-localization between LDLR and LAMP1, and by ~3 h, most of the internalized LDLR was degraded (top panel in **Fig. 6A)**. However, in berbamine-treated cells, the LDLR-antibody complex was internalized normally but failed to be sent to lysosomes for degradation (bottom panel in **Fig. 6A**).

Since the endolysosomal degradation of LDLR was compromised in the berbamine-treated cells (**Fig. 6A**), we reasoned that this should lead to an increase in the total amount of LDLR in these cells. However, we found that berbamine markedly decreased the total amount of LDLR in cells (**Fig. 6B**). We speculated that the reduced levels of LDLR that occurred in berbamine-treated cells might be due to an increase in the secretion of the endosomes containing these membrane receptors, out of cells. To verify this possibility, we quantified the concentration of extracellular vesicles (EVs) in the cell culture medium of control or berbamine-treated cells using a nanoparticle analyzer. As expected, berbamine significantly promoted the secretion of EVs **(Fig. 6C)**. We then examined whether these EVs contain elevated levels of membrane receptors in the berbamine-treated group when compared with the control group. Thus, EVs in the culture medium from the control and berbamine-treated cells were collected by ultracentrifugation, and the protein levels of several previously reported cell membrane receptors or membrane binding proteins for (+)ss RNA viruses (e.g., ITGB3 47, 48, 49, 50, 51, SCARB1 52, 53, LDLR 54, 55, 56, 57 and ANXA2 58, 59, 60), were analyzed by immunoblot analysis. We showed that the levels of LDLR, ANXA2, ITGB3, and SCARB1, similar to TSG10 (which is an exosome surface protein marker), were all markedly increased in EVs collected from the berbamine-treated cell culture medium, when compared with the control group (**Fig. 6D**). Similarly, we examined the effect of berbamine on the levels of ACE2 and DPP4 in cells and EVs. We found that when compared with the control cells, berbamine treatment markedly decreased the levels of ACE2 and DPP4 in both A549 cells (**Fig. 6E**)and Vero cells (**Fig. 6F**), but markedly increased the level of both in EVs (**Fig. 6G**). Taken together, these results suggest that berbamine inhibits the endolysosomal trafficking of the plasma membrane receptors of (+)ss RNA viruses. This leads to an increase in the level of secretion of these receptors via EVs and a concomitant decrease in the level of the receptors at the plasma membrane, thereby preventing these viruses from entering host cells.

Berbamine prevents JEV infection by inhibiting lysosomal TRPMLs. It has been previously reported that tetrandrine prevents the entry of Ebola virus into host cells by blocking two-pore channels (TPCs) 25 and TPCs has also been shown to mediate MERS-CoV pseudovirus translation 61. TPCs are Ca2+-permeable non-selective cation channels in the endo-lysosomal system 62, 63. Thus, we first examined whether

berbamine might affect the lysosomal Ca2+ levels by assessing the ability of Gly-Phe β-naphthylamide (GPN) to trigger Ca2+ release from lysosomes in cells treated with or without berbamine. We found that berbamine significantly mitigated the GPN-induced cytosolic Ca2+ increase, which suggests that it inhibits lysosomal Ca2+ channels (**Fig. 7A**). However, Ned-19, an antagonist of nicotinic acid adenine dinucleotide phosphate (NAADP), which can inhibit NAADP-mediated Ca2+ release from lysosomes or endosomes via TPCs 64, failed to inhibit ZIKV infection in A549 cells (**Fig. S5A**). We also knocked down the expression of TPC1 or TPC2 in 4T1 cells (**Fig. S5B**), and found that knockdown of either TPC2 or TPC1 had little effect on JEV infection in 4T1 cells (**Figs S5C** and **S5D**). In addition, double knockdown of both TPC1 and TPC2 failed to inhibit JEV infection in 4T1 cells (**Fig. S5E**). These data indicate that berbamine does not target TPCs to inhibit flavivirus infection.

In addition to TPCs, several other ion channels in endosomes and lysosomes have been reported to modulate endolysosomal trafficking 65, 66. Among them, TRPMLs in lysosomes and endosomes play critical roles in membrane trafficking, autophagy, and exocytosis 31, 32, 67. Therefore, we assessed whether berbamine might inhibit virus infection via modulating TRPMLs. As shown in **Figure 7B**, berbamine significantly decreased the TRPML-mediated Ca2+ release from lysosomes, which was triggered by ML-SA1, a selective and potent TRPMLs agonist 68. Consistently, knockdown of TRPML2, TRPML3, or both markedly inhibited JEV infection (**Fig. 7D** and **7E**), although TRPML1 knockdown failed to affect JEV infection (**Fig. 7C**). In addition, knockdown of both TRPML2 and TRPML3 decreased the levels of LDLR and ACE2 in cells (**Fig. 7F**). Interestingly, treatment of cells with ML-SA1 reduced the ability of berbamine to decrease the LDLR levels (**Fig. 7G** and **7H**). In summary, these data suggest that berbamine compromises the endolysosomal trafficking of viral receptors via inhibition of TRPMLs, and this leads to a decrease in the levels of viral receptors for (+)ss RNA viruses, thereby preventing these virus particles from entering the host cells.

Discussion

A number of studies have shown that virus infection changes the cytosolic Ca2+ homeostasis (or the resultant Ca2+ signaling) in the host cells, not only to facilitate the entry, replication, packaging, and release of the virus, but also to inhibit the cellular immune response against virus infection 22, 23, 24, 25, 26, 27, 28, 29, 30. It has also been shown that manipulation of the intracellular Ca2+ levels or Ca2+ signals can inhibit the virus infection 23, 24, 25, 28, 30. However, blocking the general extracellular Ca2+ influx or the release of Ca2+ from the ER or mitochondria is detrimental to cells since the cytosolic Ca2+ levels or related signals are essential to almost all cellular activities. Thus, it is impractical to use general Ca2+ channel or signaling inhibitors to prevent or treat virus infection. For example, here we showed that BAPTA-AM could completely block infection of JEV and ZIKV (**Fig. 1A** and **1B**), but it is also cytotoxic. Here, we demonstrated that berbamine inhibited TRPML-mediated Ca2+ release from lysosomes and compromised the endolysosomal trafficking of membrane receptors for many (+)ss RNA viruses, thereby promoting the secretion of these trapped membrane receptors out of cells via EVs (**Figs. 5-7**). The decreased levels of viral receptors such as ACE2, DPP4 and LDLR, are likely responsible for the wide-spectrum anti-viral activity of berbamine. Notably, berbamine did not change the basal levels of cytosolic

Ca2+ (**Fig. 7A** and **7B**), and this might explain why it was only minimally cytotoxic (**Fig. 4A-4C**). Indeed, berbamine is actually an over-the-counter medicine that has been widely used to treat leukopenia in China for many years, indicating that it is safe to use in human. We also showed that berbamine protected mice from lethal challenges of JEV (**Fig. 4E** and **4F**). Thus, considering that the current COVID-19 pandemic has created a global health and economic crisis, berbamine (as a pan-anti-(+)ss RNA viral agent), might have the potential to be developed into an effective therapeutic agent for the prevention or treatment of COVID-19.

The TRPML family comprises three members: TRPML1, TRPML2 and TRPML3 69, 70, and they are permeable to variety of cations, including Ca2+, Na+, Zn2+ and Fe2+. It is known that loss-of-function mutations in TRPML1 lead to mucolipidosis type IV (ML4), a lysosomal storage disease 71, 72, 73. Among the three members, TRPML1 is ubiquitously expressed in all tissues, whereas TRPML2 and TRPML3 appear to have a more restricted pattern of expression, although they can be detected in many tissues and cell lines, including HeLa cells, A549 cells and HEK293 cells. TRPMLs are located in the membrane of early endosomes and recycling endosomes, and they are especially rich in late endosomes and lysosomes. The activation of TRPMLs via PI(3,5)P2 can trigger the release Ca2+ from endosomes and lysosomes, which participates in various endolysosomal trafficking events, including trafficking of endosomal vesicles, fusion events between late endosomes and lysosomes, and lysosome-mediated exocytosis 71, 72, 73. Here, we found that berbamine inhibited the ML-SA1-induced release of Ca2+ from lysosomes (**Fig. 7B**), which suggests that it is a TRPML inhibitor. Moreover, knockdown of TRPLM2 or TRPML3 markedly inhibited JEV infection (**Figs 7D** and **7E**), and reduced the levels of LDLR and ACE2 in cells (**Fig. 7F**). In addition, ML- SA1 reversed the reduced level of LDLR expression in berbamine-treated cells (**Fig. 7G** and **7H**). In summary, our data suggest that berbamine inhibits TRPMLs and thus compromises the endolysosomal trafficking of membrane receptors for viruses, including receptors for SarS-CoV-2 and JEV. The accumulation of endosomes leads to an increased level of secretion of these receptors via EVs and a concomitant decrease in the virus receptor levels at the plasma membrane. This decrease in the amount of virus receptors renders the cell resistant to virus infection. Therefore, TRPMLs might be potential therapeutic targets against (+)ss RNA viruses such as SARS-CoV-2.

LDLR was the first member of the LDLR family to be identified; the family is now known to also contain VLDLR, ApoER2, LRP1, LRP2, and LRP6. These family members all share several structural domains, such as LDLR repeats (for ligand binding), an EGF-like domain and a transmembrane anchor motif. The LDLR family members mainly participate in lipoprotein trafficking to maintain cholesterol homeostasis 74. LDLR has also been shown to be one of receptors for the hepatitis C virus, rhinovirus and the vesicular stomatitis virus 39, 40, 41, 42, 43. Here we found that JEV infection triggered the internalization of LDLR, and internalized LDLR exhibited strong co-localization with the viral particles (**Fig. 5E**). In addition, LDLR knockdown abolished the JEV-induced expression of JEV-NS1 in the host cells (**Figs 5D**). These data suggest that LDLR is a potential JEV receptor. However, future work is required to confirm any interaction between LDLR and the JEV-E glycoprotein, which is responsible for the virus binding to the host cells. It is also of interest to assess if other LDLR family members might be involved in JEV infection since they do share a similar ligand binding domain.

Materials And Methods

Cell culture and virus propagation- HeLa, A549, RD, Vero, BHK-21, Huh7 and 4T1 cells were maintained in DMEM (Gibco, 12800082) containing 10% fetal bovine serum (Gibco, 10500064) and 100 U/ml of penicillin/streptomycin. PC3 cells were maintained in RPMI (Gibco, 31800022) plus 10% fetal bovine serum and 100 U/ml of penicillin/streptomycin. The JEV SA14-14-2 strain and DENV-3 were amplified from BHK-21 cells, which were maintained in DMEM containing 2% fetal bovine serum and 100 U/ml of penicillin/streptomycin. The ZIKV PRVABC59 strain and EV71 SHZH98 were generated in A549 and Vero cells, respectively.

Immunofluorescence staining- Cells were fixed with 4% paraformaldehyde (PFA) solution, blocked with PBS containing 5% normal donkey serum and 0.3% Triton™ X- 100, and then incubated with primary antibody followed by the appropriate fluorescent secondary antibody. To label the receptors on the plasma membrane, live cells were incubated with the primary antibody in PBS (+1% BSA) on ice for 90 min, followed by incubation with the fluorescent secondary antibody on ice. Images were captured with a Carl Zeiss LSM 880 confocal microscope using a 63×oil objective lens. The primary antibodies used in these experiments are listed in Table S1.

In situ RNA hybridization- In situ RNA hybridization was performed with an RNAscope® Multiplex Fluorescent kit (Advanced Cell Diagnostics, 320851) by following the manufacturer's instructions. In brief, cells attached to coverslips were fixed with 4% PFA, and then they were incubated with a specific RNA probe targeting the JEV (ACD, 435551) or ZIKV (ACD, 463781) viral genome for 2 h at 40°C. Then, up to four signal amplification systems were used to detect the target RNA. After RNA hybridization, the cells were subjected to immunofluorescence staining, as described above.

Western blot analysis- The Bradford assay (Bio-RAD) was performed to measure the protein concentration of cell lysates. An equal amount of protein sample was loaded onto 8%-12% SDS-PAGE gels for electrophoresis. The proteins were then transferred to a PVDF membrane (Millipore), blocked with 5% non-fat milk, and blotted with primary and secondary antibodies. The primary antibodies used for immunoblotting are listed in Table S2.

Cytotoxicity assay- BHK-21, Huh7, A549, HeLa, or Vero cells, which had been plated in 96-well plates (Corning, 3603), were treated with different concentrations of berbamine or tetrandrine (Santa Cruz, sc-201492) for 24 h. The cells were then stained with propidium iodide (PI; Invitrogen, P3566) and Hoechst 33258 (Invitrogen, H3570), and images were acquired using a CellInsight CX7 High-Content Screening platform with a 10× objective lens. Quantification of the dead (PI positive) cells was performed with HCS Studio™ 3.0 (Thermo Fisher) and the half maximal inhibitory concentration (IC50) was calculated via Graphpad Prism 5.

The anti-virus activity of drugs- A549 cells were pre-treated with the concentrations of chemicals indicated in the Results, for 1 h, and infected with ~1 MOI of JEV or ZIKV. At 48 h post-infection, cells were fixed with 4% PFA, stained with an anti-dsRNA antibody, and subjected to the high content screening

platform for the acquisition of fluorescence images. The percentage of infected cells was determined using HCS Studio™ 3.0., and the concentration for 50% of maximal effect (EC50) was calculated with Graphpad Prism 5. For EV71, 10 MOI of virus was used to infect RD cells and cells were fixed at 10 h post-infection.

For anti-SARS-CoV-2 activity of berbamine, VeroE6 cells were pre-treated with berbamine at a titration of different concentrations (0-75 μM) for 6 hours. Then, the cells were washed with PBS and inoculated with SARS-CoV-2 at 0.01 MOI for 2 hours. At 2 hours post infection (hpi), the cells were washed with PBS and treated with berbamine at a titration of different concentrations (0-75 μM). At 24 hpi, 100 μL of viral supernatant was lysed and proceed to total RNA extraction using the QIAamp viral RNA mini kit (Qiagen, Hilden, Germany). The extracted RNA was then used to quantify the replication of SARS-CoV-2 using real-time quantitative RT-PCR (qRT- PCR) as described previously 75.

Purification of extracellular vesicles from the culture medium- A549 cells or HeLa cells were grown in 15-cm dishes to ~80% confluency. The cells were then rinsed with PBS and incubated in EV-depleted complete medium containing DMSO or berbamine (25 μM) for 48 h. The supernatant was then collected and subjected to sequential centrifugation steps at different centrifugal forces (g) to remove the intact cells, dead cells or cell debris. After each centrifugation, the supernatant was transferred into a new 50 mL tube and the pellet was discarded. Finally, the supernatant was subjected to ultracentrifugation at 120,000 × g for 90 min, and the pellet (now containing the extracellular vesicles) was washed with PBS and subjected to another ultracentrifugation at 120,000 × g for 90 min. Finally, the exosome pellet collected and used for immunoblot analysis.

Intracellular Ca2+ measurements- HeLa cells were grown in 24-well plates to ~80% confluency. The cells were then loaded with HBSS (Gibco, 14025092) containing 4 μM Fura-2 AM (Invitrogen, F1221) and 0.4% Pluronic™ F-127 (Invitrogen, P3000MP) at room temperature for 30 min. The cells were then washed with Ca2+-free HBSS containing 2 mM EGTA and incubated in Ca2+-free HBSS in the presence or absence of berbamine (10 μM) at room temperature for another 30 min. Fluorescence images were acquired at 3 s intervals by alternate excitation at 340 nm and 380 nm with emission at 510 nm using a Nikon Eclipse Ti-S Calcium imaging system. Approximately 1 min after live cell imaging, 200 μM GPN (Abcam, ab145914) or 25 μM ML-SA1 (Tocris Bioscience, 4746) was added to the cells to trigger Ca2+ release from the lysosomes.

Small interference RNA (siRNA)- Cells were transfected with siRNAs against respective genes (**Table S3**) using Lipofectamine 3000 according to the manufacturer's instructions. The knockdown efficiency was validated by immunoblot analysis or qRT- PCR.

Anti-JEV activity of berbamine in mice- The anti-JEV activity of berbamine was performed in BALB/c mice as described previously 76. Briefly, 3 to 4-week BALB/c mice were randomly divided into four groups (eight mice per group): an uninfected and PBS-treated group, an uninfected and berbamine-treated group, a JEV-infected and PBS-treated group, and a JEV-infected and berbamine-treated group. Mice were first injected intraperitoneally with PBS or 15 mg/kg of body weight of berbamine, and 6 h later, mice were

infected intraperitoneally with 10^7 TCID50 of JEV (SA14 virus strain). Thereafter, mice were treated with PBS or berbamine (15 mg/kg) twice per day for 14 days. The mice were monitored daily for morbidity and mortality. The mice that showed severe neurological signs of disease were euthanized. All animal studies were performed in B3 level laboratories by strictly following the safety and animal ethical guidelines of university and government.

Statistical analysis- Data are presented as mean ± S.E.M. Statistically significant differences were determined by the Student's t-test and $P < 0.05$ was considered to be statistically significant.

Abbreviations

Berbamine (BBM); severe acute respiratory syndrome coronavirus 2 (SARS-CoV-2); Japanese encephalitis virus (JEV); Zika virus (ZIKV); Degus virus (DENV); Coronavirus (CoV); positive-sense single-stranded RNA viruses ((+)ss RNA viruses).

Declarations

ACKNOWLEDGEMENT

We thank members of Yue lab for their advice on the preparation of this manuscript. This work was supported by CAS-Croucher Funding Scheme, Hong Kong Research Grant Council (RGC) grants (11101717), NSFC (21778045 and 31272563), Shenzhen government research grant (JCYJ20160229165235739 and JCYJ20170413141331470), and China's sub-project of National Key R&D Program (2016YFD0500400).

CONFLICT OF INTEREST

The authors declare no conflict of interest.

References

1. Bhatt S*, et al.* The global distribution and burden of dengue. *Nature* **496**, 504 (2013).
2. Daep CA, Muñoz-Jordán JL, Eugenin Flaviviruses, an expanding threat in public health: focus on dengue, West Nile, and Japanese encephalitis virus. *Journal of neurovirology* **20**, 539-560 (2014).
3. Ghosh D, Basu A. Present perspectives on flaviviral chemotherapy. *Drug discovery today* **13**, 619-624 (2008).
4. Kok New developments in flavivirus drug discovery. *Expert opinion on drug discovery* **11**, 433-445 (2016).

5. Lee M-S, Tseng F-C, Wang J-R, Chi C-Y, Chong P, Su I-J. Challenges to licensure of enterovirus 71 vaccines. *PLoS neglected tropical diseases* **6**, (2012).

6. Smith Responding to global infectious disease outbreaks: lessons from SARS on the role of risk perception, communication and management. *Social science & medicine* **63**, 3113-3123 (2006).

7. Wang L-F, Shi Z, Zhang S, Field H, Daszak P, Eaton Review of bats and SARS. *Emerging infectious diseases* **12**, 1834 (2006).

8. Wang S-M, Liu C-C. Enterovirus 71: epidemiology, pathogenesis and management. *Expert review of anti-infective therapy* **7**, 735-742 (2009).

9. Fehr AR, Perlman Coronaviruses: an overview of their replication and pathogenesis. In: *Coronaviruses*). Springer (2015).

10. Gralinski LE, Baric RS. Molecular pathology of emerging coronavirus infections. *The Journal of pathology* **235**, 185-195 (2015).

11. Zumla A, Chan JF, Azhar EI, Hui DS, Yuen K-Y. Coronaviruses—drug discovery and therapeutic options. *Nature reviews Drug discovery* **15**, 327 (2016).

12. Ksiazek TG*, et* A novel coronavirus associated with severe acute respiratory syndrome. *New England journal of medicine* **348**, 1953-1966 (2003).

13. Shapiro M, London B, Nigri D, Shoss A, Zilber E, Fogel I. Middle East respiratory syndrome coronavirus: review of the current situation in the world. *Disaster and military medicine* **2**, 9 (2016).

14. Gubler DJ, Clark GG. Dengue/dengue hemorrhagic fever: the emergence of a global health problem. *Emerging infectious diseases* **1**, 55 (1995).

15. Al-Qahtani AA, Nazir N, Al-Anazi MR, Rubino S, Al-Ahdal Zika virus: a new pandemic threat. *The Journal of Infection in Developing Countries* **10**, 201-207 (2016).

16. Lowe R*, et al.* The Zika virus epidemic in Brazil: from discovery to future *International journal of environmental research and public health* **15**, 96 (2018).

17. Waggoner JJ, Pinsky BA. Zika virus: diagnostics for an emerging pandemic threat. *Journal of clinical microbiology* **54**, 860-867 (2016).

18. Wang H, Liang G. Epidemiology of Japanese encephalitis: past, present, and future *Therapeutics and clinical risk management* **11**, 435 (2015).

19. Campbell GL*, et* Estimated global incidence of Japanese encephalitis: a systematic review. *Bulletin of the World Health Organization* **89**, 766-774 (2011).

20. Sampath A, Padmanabhan Molecular targets for flavivirus drug discovery. *Antiviral research* **81**, 6-15 (2009).

21. Liu C-C, Tseng H-W, Wang S-M, Wang J-R, Su I-J. An outbreak of enterovirus 71 infection in Taiwan, 1998: epidemiologic and clinical manifestations. *Journal of Clinical Virology* **17**, 23-30 (2000).

22. Zhou Y, Frey TK, Yang Viral calciomics: interplays between Ca2+ and virus. *Cell calcium* **46**, 1- 17 (2009).

23. Wang S*, et al.* Screening of FDA-approved drugs for inhibitors of Japanese encephalitis virus infection. *Journal of virology* **91**, e01055-01017 (2017).

24. Scherbik SV, Brinton Virus-induced Ca2+ influx extends survival of west nile virus-infected cells. *Journal of virology* **84**, 8721-8731 (2010).

25. Sakurai Y*, et al.* Two-pore channels control Ebola virus host cell entry and are drug targets for disease treatment. *Science* **347**, 995-998 (2015).

26. Haughey NJ, Mattson Calcium dysregulation and neuronal apoptosis by the HIV-1 proteins Tat and gp120. *Journal of acquired immune deficiency syndromes (1999)* **31**, S55-61 (2002).

27. Fujioka Y*, et al.* A Ca 2+-dependent signalling circuit regulates influenza A virus internalization and infection. *Nature communications* **4**, 2763 (2013).

28. Fujioka Y*, et al.* A sialylated voltage-dependent Ca2+ channel binds hemagglutinin and mediates influenza A virus entry into mammalian cells. *Cell host & microbe* **23**, 809-818. e805 (2018).

29. Bissig C*, et al.* Viral infection controlled by a calcium-dependent lipid-binding module in *Developmental cell* **25**, 364-373 (2013).

30. Alam M*, et al.* Verapamil has Antiviral Activities that Target Different Steps of the Influenza Virus Replication Cycle. *J Antivir Antiretrovir* **8**, 121-130 (2016).

31. Wang W, Zhang X, Gao Q, Xu TRPML1: an ion channel in the lysosome. *Handb Exp Pharmacol* **222**, 631-645 (2014).

32. Venkatachalam K, Wong CO, Zhu MX. The role of TRPMLs in endolysosomal trafficking and function. *Cell Calcium* **58**, 48-56 (2015).

33. Weber F, Wagner V, Rasmussen SB, Hartmann R, Paludan Double-stranded RNA is produced by positive-strand RNA viruses and DNA viruses but not in detectable amounts by negative- strand RNA viruses. *Journal of virology* **80**, 5059-5064 (2006).

34. O'Brien CA*, et al.* Viral RNA intermediates as targets for detection and discovery of novel and emerging mosquito-borne viruses. *PLoS neglected tropical diseases* **9**, (2015).

35. Dorobantu CM*, et* Modulation of the host lipid landscape to promote RNA virus replication: the picornavirus encephalomyocarditis virus converges on the pathway used by hepatitis C virus. *PLoS pathogens* **11**, (2015).

36. Bhagya N, Chandrashekar Tetrandrine--A molecule of wide bioactivity. *Phytochemistry* **125**, 5-13 (2016).

37. Wang G, Lemos JR, Iadecola C. Herbal alkaloid tetrandrine: fron an ion channel blocker to inhibitor of tumor proliferation. *Trends Pharmacol Sci* **25**, 120-123 (2004).

38. Sakurai Y*, et* Ebola virus. Two-pore channels control Ebola virus host cell entry and are drug targets for disease treatment. *Science* **347**, 995-998 (2015).

39. Monazahian M*, et al.* Low density lipoprotein receptor as a candidate receptor for hepatitis C virus. *J Med Virol* **57**, 223-229 (1999).

40. Wunschmann S, Medh JD, Klinzmann D, Schmidt WN, Stapleton Characterization of hepatitis C virus (HCV) and HCV E2 interactions with CD81 and the low-density lipoprotein receptor. *J Virol* **74**, 10055-10062 (2000).

41. Finkelshtein D, Werman A, Novick D, Barak S, Rubinstein M. LDL receptor and its family members serve as the cellular receptors for vesicular stomatitis *Proc Natl Acad Sci U S A* **110**, 7306-7311 (2013).

42. Fischer DG, Tal N, Novick D, Barak S, Rubinstein An antiviral soluble form of the LDL receptor induced by interferon. *Science* **262**, 250-253 (1993).

43. Bochkov YA, Gern JE. Rhinoviruses and Their Receptors: Implications for Allergic Disease. *Curr Allergy Asthma Rep* **16**, 30 (2016).

44. Hoffmann M*, et* SARS-CoV-2 Cell Entry Depends on ACE2 and TMPRSS2 and Is Blocked by a Clinically Proven Protease Inhibitor. *Cell* **181**, 271-280 e278 (2020).

45. Raj VS*, et al.* Dipeptidyl peptidase 4 is a functional receptor for the emerging human coronavirus-EMC. *Nature* **495**, 251-254 (2013).

46. Powelka AM*, et al.* Stimulation-dependent recycling of integrin beta1 regulated by ARF6 and Rab11. *Traffic* **5**, 20-36 (2004).

47. Jackson T*, et al.* Arginine-glycine-aspartic acid-specific binding by foot-and-mouth disease viruses to the purified integrin alpha (v) beta3 in *Journal of Virology* **71**, 8357-8361 (1997).

48. Gianni T, Gatta V, Campadelli-Fiume G. αVβ3-integrin routes herpes simplex virus to an entry pathway dependent on cholesterol-rich lipid rafts and dynamin2. *Proceedings of the National Academy of*

Sciences **107**, 22260-22265 (2010).

49. Chu JJ-h, Ng M-L. Interaction of West Nile virus with αvβ3 integrin mediates virus entry into cells. *Journal of Biological Chemistry* **279**, 54533-54541 (2004).

50. Chu J, Ng M. Characterization of a 105-kDa plasma membrane associated glycoprotein that is involved in West Nile virus binding and infection. *Virology* **312**, 458-469 (2003).

51. Berinstein A, Roivainen M, Hovi T, Mason P, Baxt B. Antibodies to the vitronectin receptor (integrin alpha V beta 3) inhibit binding and infection of foot-and-mouth disease virus to cultured cells. *Journal of virology* **69**, 2664-2666 (1995).

52. Westhaus S*, et* Scavenger receptor class B member 1 (SCARB1) variants modulate hepatitis C virus replication cycle and viral load. *Journal of hepatology* **67**, 237-245 (2017).

53. Li Y, Kakinami C, Li Q, Yang B, Li H. Human apolipoprotein AI is associated with dengue virus and enhances virus infection through SR-BI. *PloS one* **8**, (2013).

54. Monazahian M*, et al.* Low density lipoprotein receptor as a candidate receptor for hepatitis C virus. *Journal of medical virology* **57**, 223-229 (1999).

55. Molina S*, et al.* The low-density lipoprotein receptor plays a role in the infection of primary human hepatocytes by hepatitis C virus. *Journal of hepatology* **46**, 411-419 (2007).

56. Hofer F*, et al.* Members of the low density lipoprotein receptor family mediate cell entry of a minor-group common cold virus. *Proceedings of the National Academy of Sciences* **91**, 1839- 1842 (1994).

57. Finkelshtein D, Werman A, Novick D, Barak S, Rubinstein M. LDL receptor and its family members serve as the cellular receptors for vesicular stomatitis virus. *Proceedings of the National Academy of Sciences* **110**, 7306-7311 (2013).

58. Raynor CM, Wright JF, Waisman DM, Pryzdial Annexin II enhances cytomegalovirus binding and fusion to phospholipid membranes. *Biochemistry* **38**, 5089-5095 (1999).

59. Mei M*, et al.* Identification of novel viral receptors with cell line expressing viral receptor- binding protein. *Scientific reports* **5**, 7935 (2015).

60. Gonzalez-Reyes S*, et al.* Role of annexin A2 in cellular entry of rabbit vesivirus. *Journal of general virology* **90**, 2724-2730 (2009).

61. Gunaratne GS, Yang Y, Li F, Walseth TF, Marchant JS. NAADP-dependent Ca(2+) signaling regulates Middle East respiratory syndrome-coronavirus pseudovirus translocation through the endolysosomal system. *Cell Calcium* **75**, 30-41 (2018).

62. Grimm C, Chen CC, Wahl-Schott C, Biel M. Two-Pore Channels: Catalyzers of Endolysosomal Transport and Function. *Front Pharmacol* **8**, 45 (2017).

63. Patel S. Function and dysfunction of two-pore channels. *Sci Signal* **8**, re7 (2015).

64. Naylor E*, et al.* Identification of a chemical probe for NAADP by virtual screening. *Nat Chem Biol* **5**, 220-226 (2009).

65. Abe K, Puertollano Role of TRP channels in the regulation of the endosomal pathway.m*Physiology (Bethesda)* **26**, 14-22 (2011).

66. Grimm C, Bartel K, Vollmar AM, Biel Endolysosomal Cation Channels and Cancer-A Link with Great Potential. *Pharmaceuticals (Basel)* **11**, (2018).

67. Cheng X, Shen D, Samie M, Xu Mucolipins: Intracellular TRPML1-3 channels. *FEBS Lett* **584**, 2013-2021 (2010).

68. Feng X, Xiong J, Lu Y, Xia X, Zhu MX. Differential mechanisms of action of the mucolipin synthetic agonist, ML-SA1, on insect TRPML and mammalian TRPML1. *Cell Calcium* **56**, 446- 456 (2014).

69. Zeevi DA, Frumkin A, Bach G. TRPML and lysosomal function. *Biochimica et Biophysica Acta (BBA)-Molecular Basis of Disease* **1772**, 851-858 (2007).

70. Bach G. Mucolipin 1: endocytosis and cation channel—a *Pflügers Archiv* **451**, 313-317 (2005).

71. Sun M*, et* Mucolipidosis type IV is caused by mutations in a gene encoding a novel transient receptor potential channel. *Human molecular genetics* **9**, 2471-2478 (2000).

72. Berman E, Livni N, Shapira E, Merin S, Levij I. Congenital corneal clouding with abnormal systemic storage bodies: a new variant of *The Journal of pediatrics* **84**, 519-526 (1974).

73. Bargal R*, et al.* Identification of the gene causing mucolipidosis type *Nature genetics* **26**, 118-122 (2000).

74. Go GW, Mani A. Low-density lipoprotein receptor (LDLR) family orchestrates cholesterol homeostasis. *Yale J Biol Med* **85**, 19-28 (2012).

75. Chu H*, et* Comparative replication and immune activation profiles of SARS-CoV-2 and SARS- CoV in human lungs: an ex vivo study with implications for the pathogenesis of COVID-19. *Clin Infect Dis*, (2020).

76. Wei J-c*, et al.* Design and evaluation of a multi-epitope peptide against Japanese encephalitis virus infection in BALB/c *Biochemical and biophysical research communications* **396**, 787- 792 (2010).

Figures

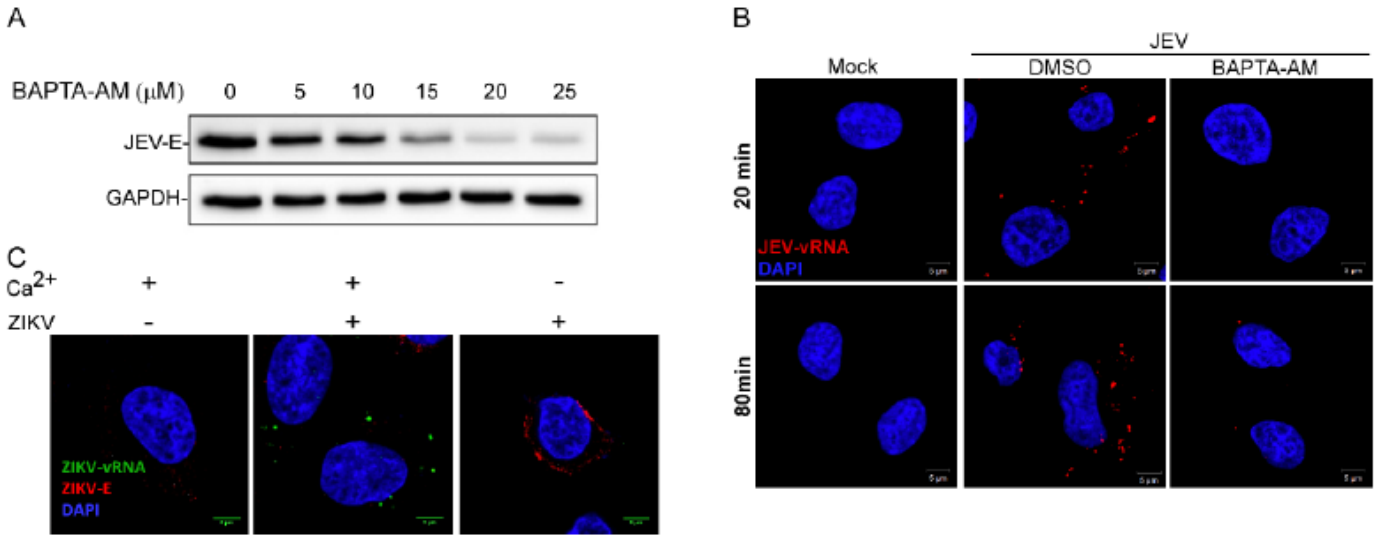

Figure 1

Calcium signaling is required for flavivirus infection. (A) A549 cells were treated with the indicated doses of BAPTA-AM for 1 h, and then they were infected with ~10 MOI of JEV for 10 h. Cell lysates were collected and subjected to immunoblot analysis for viral protein levels. (B) A549 cells were treated with DMSO, BAPTA-AM (20 μM) for 1 h and then incubated with ~50 MOI of JEV on ice for 1h. Afterwards, the cells were placed on 37°C for either 20 min or 80 min, followed by in situ RNA hybridization for detecting the RNA genome (red) of JEV. (C) A549 cells were incubated with ~50 MOI of ZIKV on ice for 1 h and then cells were incubated in HBSS ± Ca2+ at 37°C for 1 h followed by in situ RNA hybridization and ZIKV-E immunostaining.

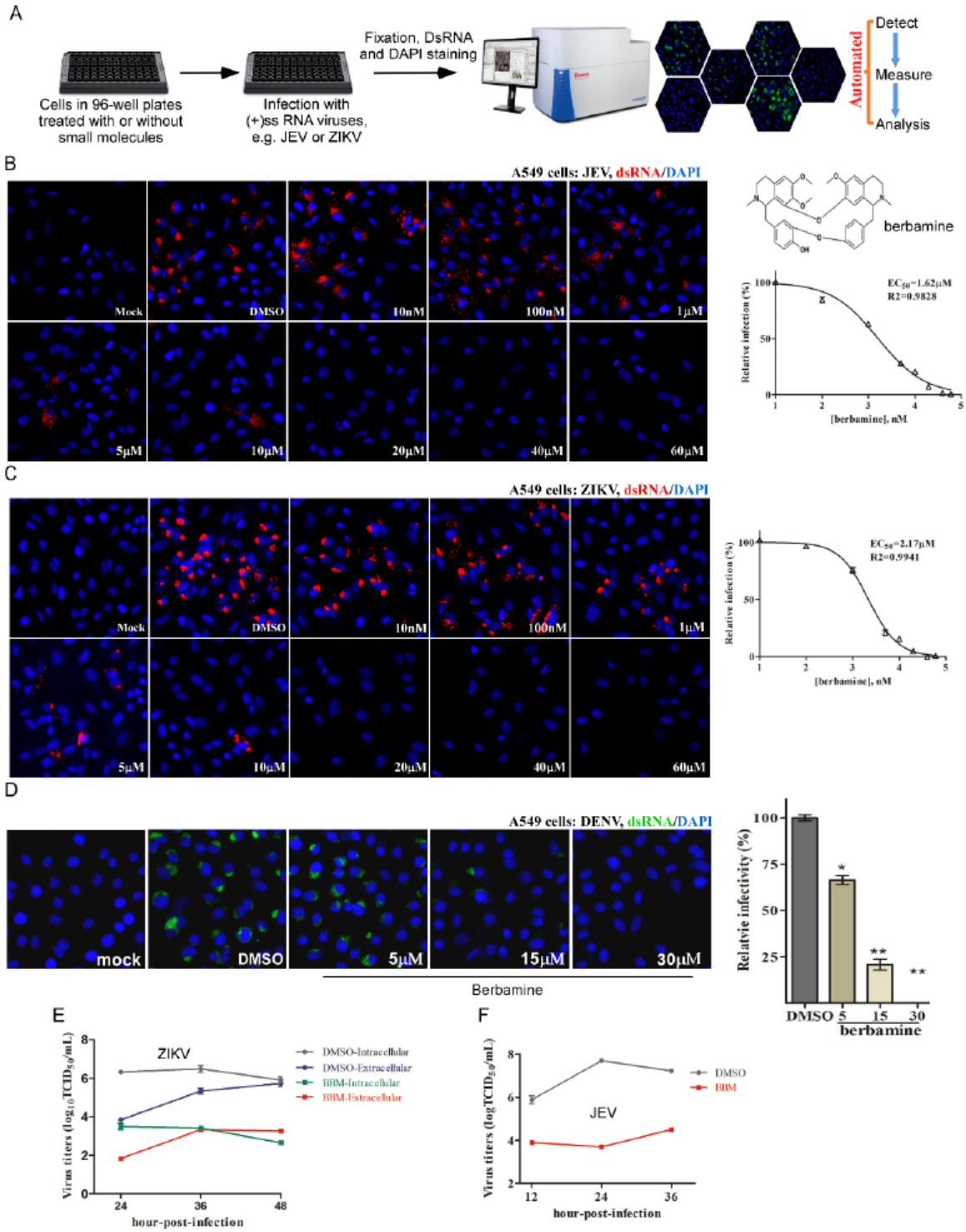

Figure 2

Berbamine inhibits JEV, ZIKV or DENV infection of host cells. (A) The high-content image platform used to screen anti-viral agents. (B-D) A549 cells were treated with DMSO or berbamine at different concentrations for 1 h, and then infected with ~1 MOI JEV (B), ZIKV (C), or DENV (D) for 48 h. The cells were the immunolabeled with dsRNA antibodies and subjected to fluorescence imaging. (E) Pretreatment of A549 cells with berbamine (40 μM) significantly inhibited JEV progeny virion production, as

determined by virus titer measurements. (F) Pretreatment of A549 cells with berbamine (20 μM) significantly inhibited ZIKV intracellular and extracellular viral production as determined by virus titer measurements.

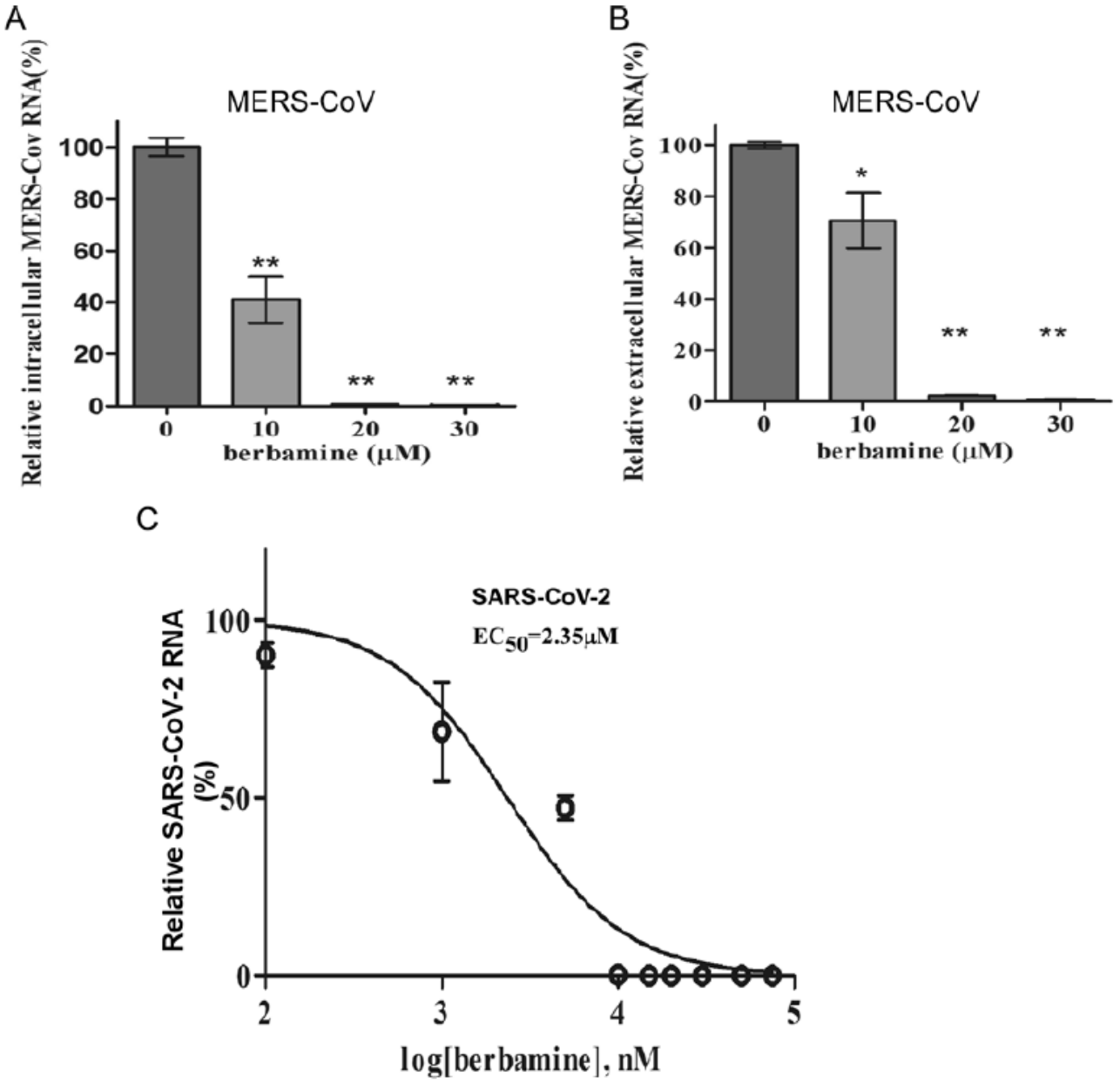

Figure 3

Berbamine inhibits MERS-CoV or SARS-CoV-2 infection of host cells. (A, B) Primary human lung fibroblast cells were treated with berbamine at the indicated concentration for 3 h, after which they were infected with MERS-CoV. Supernatant (A) and cell lysate (B) were collected separately and subjected to RT-PCR quantification of MERS-CoV RNA. (C) VeroE6 cells were treated with berbamine at the indicated concentrations for 3 h, and then they were then infected with SARS-CoV-2. The cell lysates were collected and subjected to RT-PCR quantification of SARS-CoV-2 RNA.

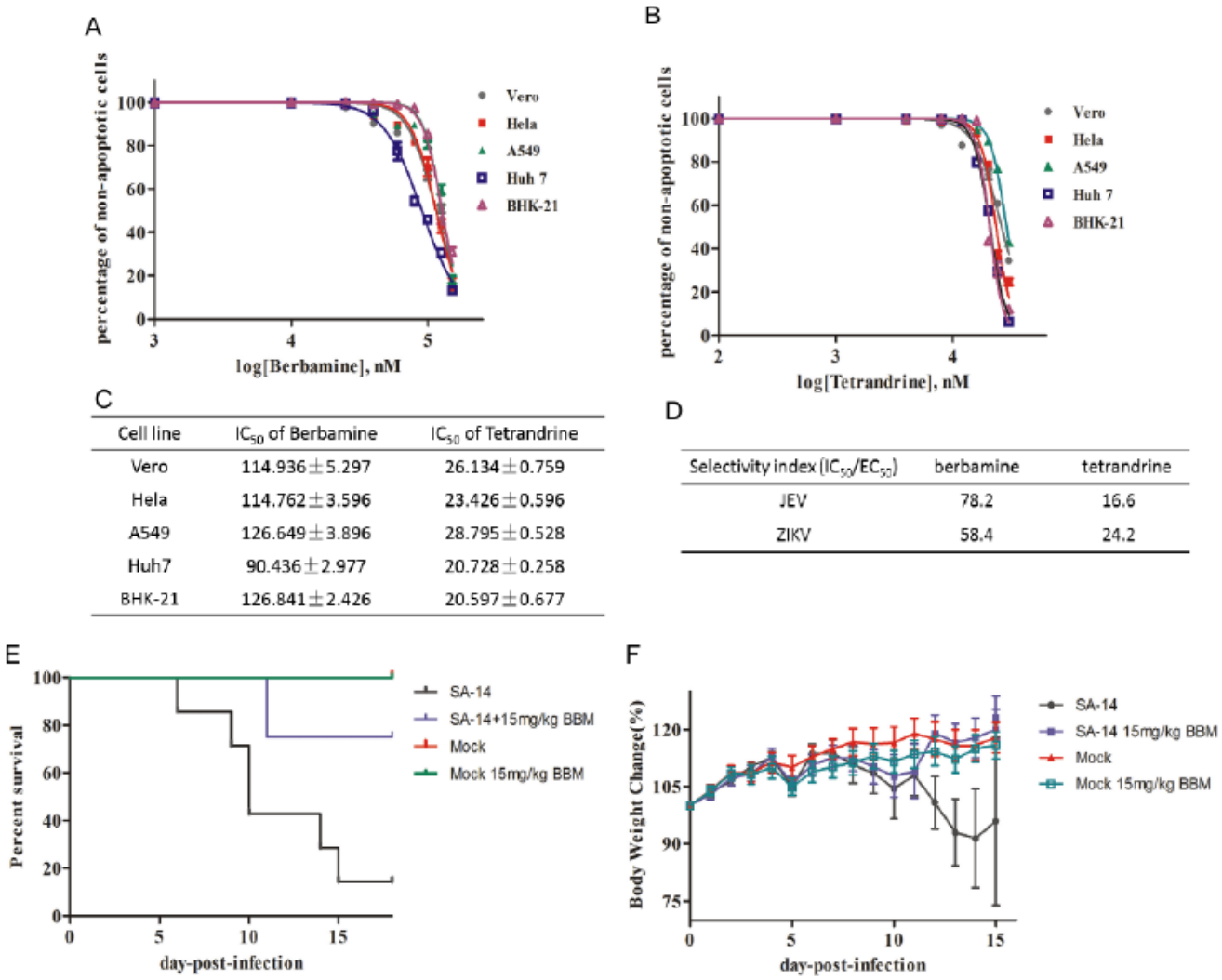

C

Cell line	IC_{50} of Berbamine	IC_{50} of Tetrandrine
Vero	114.936±5.297	26.134±0.759
Hela	114.762±3.596	23.426±0.596
A549	126.649±3.896	28.795±0.528
Huh7	90.436±2.977	20.728±0.258
BHK-21	126.841±2.426	20.597±0.677

D

Selectivity index (IC_{50}/EC_{50})	berbamine	tetrandrine
JEV	78.2	16.6
ZIKV	58.4	24.2

Figure 4

Berbamine protects mice from a lethal challenge of JEV. (A, B) Cells grown in 96-well plates were treated with different concentrations of berbamine (A) or tetrandrine (B) for 48 h and then they were subjected to PI and Hoechst staining. Images were acquired and PI-positive cells were quantified. (C) The IC50 values of berbamine and tetrandrine in different cell lines. (D) The SI of berbamine and tetrandrine against ZIKV or JEV infections. (E) The survival rate of mice infected with the 10^7 TCID_50 SA-14 JEV strain treated with or without 15 mg/kg berbamine. Mice treated with berbamine without infection were used as a control to monitor the side effects of berbamine. (F) The body weight change of mice infected with the 10^7 TCID_50 SA-14 JEV strain treated with or without 15mg/kg berbamine.

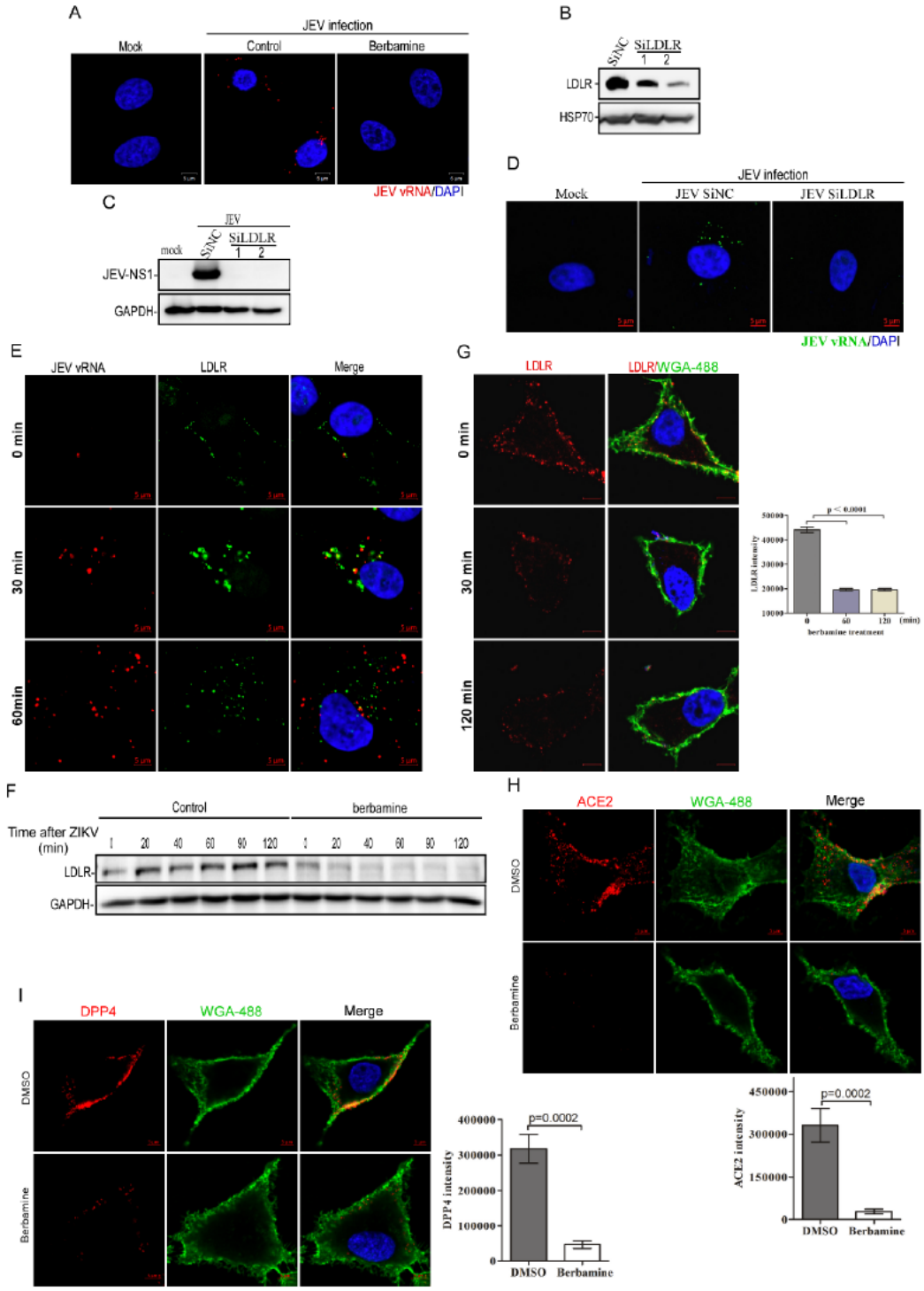

Figure 5

Berbamine prevents the entry of (+)ss RNA virus by depleting their plasma membrane receptor(s) in host cells. (A) A549 cells were treated with berbamine (20 μM) for 1 h, and were then incubated with ~50 MOI JEV on ice for 1 h. Afterwards, they were incubated in medium at 37˚C for another 80 min followed by in situ RNA hybridization to detect the RNA genome (red) of JEV. (B) Knockdown of LDLR in A549c cells by siRNAs. (C, D) A549 cells were transfected with siRNAs against LDLR, and were then infected with JEV for

24 h followed by immunoblot analysis against JEV-NS1 (C) or in situ RNA hybridization to detect the RNA genome (green) of JEV (D). (E) A549 cells were incubated with an anti-LDLR primary antibody and an Alexa Fluor 488-tagged secondary antibody (green) on ice, before being infected with ~50 MOI of JEV on ice. Subsequently, the cells were incubated at 37˚C for indicated times, followed by in situ RNA hybridization for detecting the JEV RNA genome (red). (F) A549 cells were treated with/without berbamine for 1 h, and then they were incubated with JEV on ice for 1 h. The cells were then incubated at 37˚C for the indicated times followed by LDLR immunoblot analysis. (G-I) A549 cells were treated with/without berbamine (50 μM) for the indicated times, followed by immunostaining of LDLR (G), ACE2 (H), or DPP4 (I). Alexa Fluor® 488-conjugated wheat germ agglutinin (WGA) was used to label the plasma membrane.

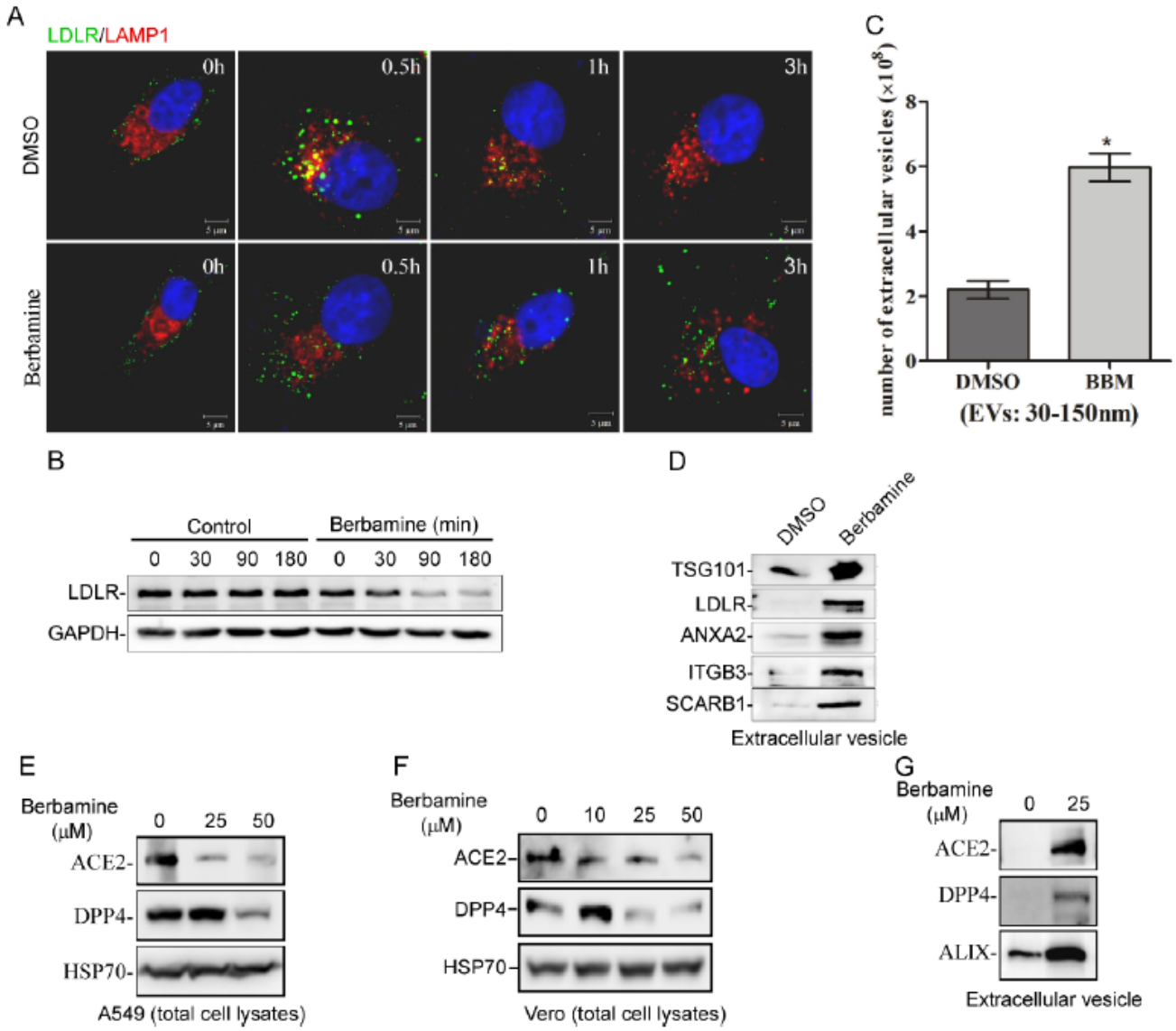

Figure 6

Berbamine inhibits endolysosomal trafficking and induces the secretion of extracellular vesicles to decrease the level of receptors at the plasma membrane. (A) A549 cells were treated with/without berbamine (50 μM) for 1 h, after which they were immunolabeled with and anti-LDLR primary antibody and the appropriate secondary antibody on ice. Afterwards, cells were incubated at 37˚C for the indicated times, followed by LAMP1 immunostaining. (B) A549 cells were treated with/without berbamine (50 μM) for the indicated times, and cell lysates were then subjected to LDLR immunoblotting analysis. (C, D) EVs were collected from the culture medium of control or berbamine-treated A549 cells, and their concentration and distribution of sizes were determined with a nanoparticle tracking analyzer (C). The levels of TSG101, LDLR, ANXA2, ITGB3 and SCARB1 in these EVs were determined by immunoblot analysis (D). (E, F) A549 cells (E) or Vero cells (F) in the presence of cycloheximide (7.5 mg/ml) were treated with/without berbamine (50 μM) for 6 h, after which the cell lysates were subjected to ACE2 or DPP4 immunoblot analysis. (G) EVs were collected from the culture medium of control or berbamine-treated A549 cells, and the levels of ACE2, DPP4, and ALIX in these EVs were determined by immunoblot analysis.

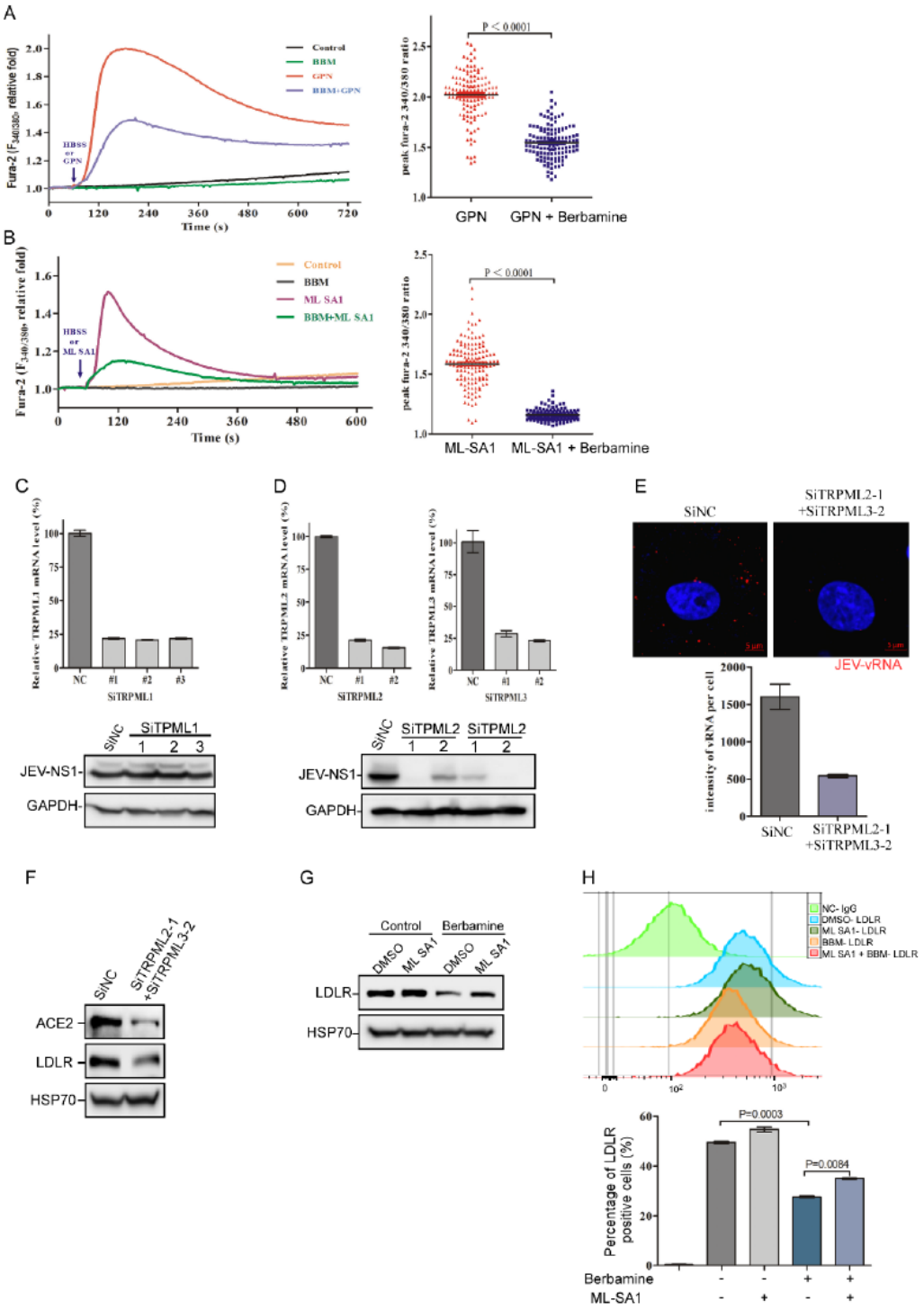

Figure 7

Berbamine inhibits JEV infection by blocking TRPMLs. (A, B) Berbamine (BBM) significantly inhibited the GPN- (A) or ML-SA1- (B) induced cytosolic Ca2+ increase in Fura-2-loaded HeLa cells. (C) A549 cells were transfected with siRNAs against TRPML1, and were then infected with JEV for 24 h followed by immunoblot analysis against JEV-NS1. TRPML1 knockdown efficiency was verified by qRT-PCR. (D) A549 cells were transfected with siRNAs against TRPML2 or TRPML3, and were then infected with JEV for 24 h

followed by immunoblot analysis against JEV-NS1. TRPML2 or TRPML3 knockdown efficiency was verified by qRT- PCR. (E) A549 cells were transfected with siRNAs against TRPML2 and TRPML3, and were then infected with ~50 MOI JEV for 90 min followed by in situ RNA hybridization to detect the RNA genome (red) of JEV. (F) A549 cells were transfected with siRNAs against TRPML2 and TRPML3, followed by immunoblot analysis against ACE2 and LDLR. (G, H) A549 cells in the presence or absence of ML-SA1 were treated with/without berbamine for 3 h, followed by LDLR immunoblot analysis (G). Alternatively, the live cells were immunolabeled with the anti-LDLR antibody, followed by FACS analysis to measure the cell surface LDLR levels (H).

Supplementary Files

This is a list of supplementary files associated with this preprint. Click to download.

- Supplementalinformation.pdf